2013 IEEE/RSJ International Conference on
Intelligent Robots and Systems (IROS)
November 3-7, 2013. Tokyo, Japan

Variable Impedance Control with an Artificial Muscle Manipulator Using Instantaneous Force and MR Brake

H. Tomori, S. Nagai, T. Majima and T. Nakamura, Member, IEEE

Abstract — **Highly rigid actuators such as geared motors or hydraulic actuators are widely used in industrial robots. To obtain high-speed motion, it is necessary to increase the actuator output as the robot weight increases. In contrast, humans perform motions using instantaneous force, such as jumping or throwing, via variable stiffness characteristics. We have developed a one-degree-of-freedom manipulator with a variable rheological joint using a straight-fiber-type artificial muscle and a magnetorheological (MR) brake. With the generation of instantaneous force, the dead and rise times decreased compared to the conventional method. After the generation of an arbitrary instantaneous force, we were able to control the robot's arm position by applying an equilibrium force on the joint. Furthermore, we were able to control the vibrations of the arm by controlling the MR brake using an evaluation function.**

I. Introduction

Highly rigid actuators such as geared motors or hydraulic actuators are widely used in industrial robots. To obtain high-speed motion, it is necessary to increase the actuator output as the robot weight increases.

In contrast, humans perform motions such as jumping and throwing using their muscles and instantaneous force. This instantaneous force is created by a high-speed change in muscle stiffness, which changes the potential energy in the muscles to kinetic energy. Therefore, systems require high compliance and a high-speed stiffness change to generate instantaneous force, which is difficult to achieve with highly rigid actuators. In addition, improved instantaneous motions are achieved by adequately controlling variable impedance [1].

To generate instantaneous force, we have developed a straight-fiber artificial muscle [2]–[5] as a variable elasticity actuator. This artificial muscle has a high contraction percentage, high contractive force, and a long lifespan compared to the McKibben-type rubber artificial muscle [6], [7]. Moreover, the artificial muscle is lightweight and flexible and delivers high output.

Furthermore, we used a magnetorheological (MR) fluid brake. The MR fluid is a functional fluid whose apparent viscosity can be changed reversibly at high speeds by applying a magnetic field [10]. Although the MR brake is a friction damper, it can be used as a variable viscosity damper by controlling its apparent viscosity. Therefore, we used this device as a friction damper to generate instantaneous force with a high-speed change in stiffness and as a variable viscosity damper to control the vibration of motion.

In previous studies, Floreano [8] developed a miniature jumping robot using a motor and a spring. However, the elastic coefficient of the actuator used was constant, and the instantaneous force and position could not be controlled independently. Although Niiyama [9] developed a jumping robot using the McKibben artificial muscle, the jumping operation of this robot was designed by trial and error, and the air-pressure-control capabilities were inadequate. Furthermore, previous studies have not allowed for viscosity control, and the control of the motion generated by instantaneous force has not been sufficiently developed.

Therefore, we propose the generation of instantaneous force via a high-speed variable stiffness change in artificial muscles and MR brakes in a manipulator joint. Furthermore, we control the manipulator arm position by applying an equilibrium force to the joint. We also control the vibration of the arm using the MR brake as a variable viscosity damper. These methods enable us to independently control the speed, position, and vibration of the arm.

In this paper, we propose a method for generating instantaneous force with a one-degree-of-freedom (1DOF) manipulator using artificial muscles and an MR brake in the joint and validate this proposed method experimentally and via simulation. Next, we control the arm position by increasing the stiffness of the joint. Then, we propose a viscosity controller for the MR brake using an evaluation function for vibration control. To design this controller, we used a nonlinear dynamic characteristics model of the manipulator.

II. 1DOF Manipulator with Variable Rheological Joint

A. Straight-Fiber-Type Artificial Muscle

The developed in our laboratory has a tubular shape and is made of natural rubber latex. Fig. 1 shows a schematic of the

H. Tomori is with the Faculty of Science and Engineering, Department of Precision Mechanics Chuo University 1-13-27 Kasuga, Bunkyo-ku, Tokyo 112-8551, Japan (corresponding author: 81-3-3817-1825; fax: 81-3-3817 -1820; e-mail: h_tomori@bio.mech.chuo-u.ac.jp).

S. Nagai is with the Faculty of Science and Engineering, Department of Precision Mechanics Chuo University 1-13-27 Kasuga, Bunkyo-ku, Tokyo 112-8551, Japan (e-mail: s_nagai@bio.mech.chuo-u.ac.jp).

T. Majima is with the Faculty of Science and Engineering, Department of Precision Mechanics Chuo University 1-13-27 Kasuga, Bunkyo-ku, Tokyo 112-8551, Japan (e-mail: t_majima@bio.mech.chuo-u.ac.jp).

T. Nakamura is with Chuo University 1-13-27 Kasuga, Bunkyo-ku, Tokyo 112-8551, Japan (e-mail: nakamura@mech.chuo-u.ac.jp).

978-1-4673-6357-0/13/$31.00 ©2013 IEEE

artificial muscle. The muscle structure includes a lengthwise carbon fiber layer. Consequently, when air pressure is applied to the muscle, it expands in the radial direction and contracts lengthwise. The contractile force is then used as an actuator. The artificial muscle is flexible and lightweight and provides high output. Furthermore, its elasticity changes with the applied air pressure.

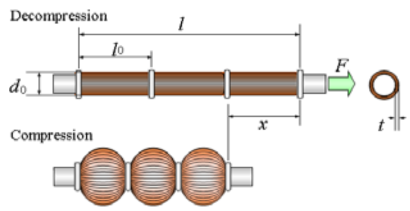

Figure 1. Schematic of fiber-double-layer-type artificial muscle

B. MR Fluid Brake

To generate instantaneous force, a rapid change in stiffness is required. Therefore, we focused on the MR fluid brake. By applying a magnetic field, the apparent viscosity of the MR fluid can be changed in several milliseconds. This device has a friction damper function that can be used for a high-speed change in the stiffness of the manipulator joint. In addition, it can be used as a variable viscosity damper to control the arm's vibration by controlling its apparent viscosity.

In this study, we used an MRB-2107-3 (LORD Co.) MR fluid brake. Fig. 2 illustrates MRB-2107-3, and Table 1 gives its specifications. The MR fluid in this device generates friction on the disk surface by the magnetic field. Thus, this mechanism can halt the arm's rotation.

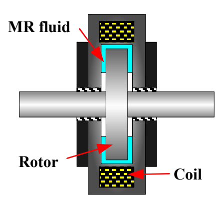

Figure 2. Configuration of MR brake

TABLE I. SPECIFICATION OF MR BRAKE

Term	Parameter
Diameter (mm)	92.2
Width (mm)	36.6
Weight (kg)	1.4
Maximum torque (Nm)	7
Minimum torque (Nm)	< 0.34
Max current value (A)	1

C. 1DOF Manipulator

Fig. 3 shows the developed 1DOF artificial muscle manipulator. In this manipulator, two artificial muscles are arranged in parallel. The belt pulley transmits the contractive force of the artificial muscles to the rotation axis. The MR brake is fixed to the first joint through a gear. As a result, it is possible to apply a brake to the rotation axis.

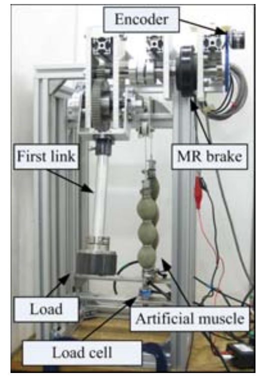

Figure 3. 1DOF artificial muscle manipulator

D. Function of the manipulator

This manipulator has variable stiffness, viscosity, and elasticity in its joint. Thus, the manipulator can perform the following tasks:

- The manipulator independently controls the arm position and joint stiffness by controlling the elasticity of each muscle.
- It halts the arm motion using the MR brake as a friction damper. Elastic energy can be accumulated in the muscle by increasing its elastic force (i.e., by applying the brake). By quickly releasing the brake, the manipulator generates instantaneous force from the accumulated elastic energy.
- Elastic energy can also be accumulated by increasing the stiffness of the joint using both muscles, which have an opposing relationship. Thus, the manipulator generates kinetic energy by changing the equilibrium of the contractile force of muscles.
- The MR brake can be used as a variable viscosity damper by controlling its apparent viscosity. It can control the vibration of the arm.

In this paper, we explain the second task in section IV, the first task in section V, and the fourth task in section VI.

III. NONLINEAR DYNAMIC CHARACTERISTICS MODEL OF THE MANIPULATOR

A. Outline of the Manipulator Model

We built a manipulator model taking the dynamic characteristics of the artificial muscle into account. This manipulator model allows for an analytical approach to the control problem.

Fig. 4 shows the schematic of the model, which consists of three parts. The first part is a mechanical equilibrium model [3], [5] that treats the static characteristics of the muscle. With this model, the relationships between pressure, load, and contraction are linearized. The second part is a model containing elements related to the dynamic characteristics of the air muscle system, including a pressure valve [11]–[13]. The third part is a manipulator load system model. We combined these three parts into one manipulator model.

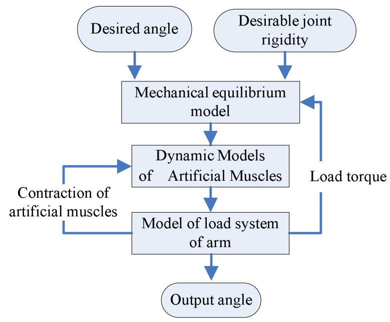

Figure 4. Schematic of the manipulator

B. Mechanical Equilibrium Model

In this section, we describe the mechanical equilibrium model that treats the static characteristics of the manipulator [3], [5]. The artificial muscles are difficult to control because they are highly nonlinear in contraction, contractile force, and pressure. Therefore, we used a mechanical equilibrium model to control the artificial muscle. Through this mechanical equilibrium model, the internal pressures P_1 and P_2 [MPa] of an artificial muscle can be calculated from the joint rigidity K_j [Nm/rad], load torque τ_l [Nm], and target angle θ_d of the arm [rad].

In the calculations, α is the constant that approximates the relationship between the extent of contraction and diameter, l_0 is the initial length [m], d_0 is the initial diameter [m], K is the elastic coefficient [N/m^2], K_a is a coefficient between pressure and spring constant of an artificial muscle [N/(m.MPa)], t is the thickness of the rubber [m], M is the coefficient of the fiber of artificial muscle, n is the number of fibers, b is the width of the fiber [m], Ψ is angle slack of wire [rad], and r_p is the pulley radius [m].

$$P_1(\theta_d,\tau) = [G_{11}(\phi_{01})G_{22}(\phi_{02}) - G_{12}(\phi_{02})G_{21}(\phi_{01}) + \frac{K_j}{K_{a2}} G_{21}(\phi_{01})G_{32}(\phi_{02}) + \frac{\tau}{r_p} G_{21}(\phi_{01})G_{22}(\phi_{02})] / [G_{22}(\phi_{02})G_{31}(\phi_{01}) + \frac{K_{a1}}{K_{a2}} G_{21}(\phi_{01})G_{32}(\phi_{02})] \quad (1)$$

$$P_2(\theta_d,\tau) = \frac{K_j}{K_{a2}} - \frac{K_{a1}}{K_{a2}} P_1 \quad (2)$$

$$G_{1i}(\phi_{0i}) = \frac{2K_i t_i}{d_{0i}} \left[\frac{l_{0i}}{d_{0i}}\right]^2 \left[\frac{\sin\phi_{0i} - \phi_{0i}\cos\phi_{0i}}{\phi_{0i}^{\ 2}}\right] \quad (3)$$

$$G_{2i}(\phi_{0i}) = \frac{M\tan\phi_{0i}}{d_{0i} n b_i} \quad (4)$$

$$G_{3i}(\phi_{0i}) = \left[\frac{l_{0i}}{d_{0i}}\right]^2 \left[\frac{\phi_{0i} - \sin\phi_{0i}\cos\phi_{0i}}{\phi_{0i}^{\ 2}}\right] + 2\frac{l_{0i}}{d_{0i}}\frac{\sin\phi_{0i}}{\phi_{0i}} - \frac{\pi d_{0i} M}{4nb_i}\tan\phi_{0i} \quad (5)$$

$$\phi_{0i} = \frac{2\alpha_i l_{0i}^{\ 1.5} x_{di}^{\ 0.5}}{(l_{0i} - x_{di})^2 + \alpha_i^{\ 2} x_{di} l_{0i}} \qquad (\alpha = 1.4) \quad (6)$$

$$x_{d1} = \frac{r_p\psi_1 - r_p\theta_d}{3} \quad (7)$$

$$x_{d2} = \frac{r_p\psi_2 + r_p\theta_d}{3} \quad (8)$$

C. Dynamic Characteristics Model of the Artificial Muscle

This section describes the dynamic characteristics model of the artificial muscle. In this model, the input is the target pressure from the control part, and the output is the contractile force of the artificial muscle. The flowchart of this model is shown in Fig. 5. Elements related to the dynamic characteristics of the artificial muscle include the speed response of the solenoid valve, ease of passing air in the air tube, and pressure and volume changes.

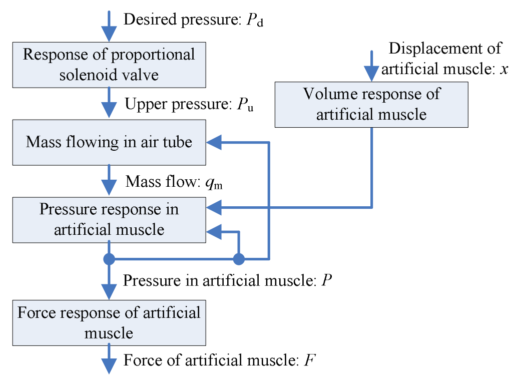

Figure 5. Nonlinear model of the straight-fiber-type artificial muscle

1) Speed response of the solenoid valve

First, we obtained the speed response of the solenoid valve experimentally and concluded that it followed a second-order lag system with a dead time. The characteristics of the solenoid valve are shown in equation (9), where $T_1 = 0.025$ [s], $T_2 = 0.025$ [s], and $L_d = 0.040$ [s]:

$$G(s) = \frac{1}{T_1 s + 1}\frac{1}{T_2 s + 1} e^{-sL_d} \approx \frac{1}{T_1 s + 1}\frac{1}{T_2 s + 1}\frac{s^2 - 150s + 7500}{s^2 + 150s + 7500} \quad (9)$$

2) Air pressure propagation in a pipeline

Next, we constructed a model of the air tube that transmits pressure from the solenoid valve to the artificial muscles. The whole system, which includes the air tube and the inside of the solenoid valve, is expressed using the sonic conductance C, according to JIS B 8390 [14]. When the internal pressures of the artificial muscle and solenoid valve are determined, the mass flow rate of the air that flows into the inside of the artificial muscle, i.e., q_m [Kg/s], is given by equations (10) and (11). We determined the sonic conductance experimentally:

$$0.528 < P/P_u \le 1$$

$$q_m(P_u, P) = C p_u \rho_0 \sqrt{\frac{T_0}{T_u}} \sqrt{1 - \left(\frac{P/P_u - \gamma}{1-\gamma}\right)} \quad (10)$$

$$0 < P/P_u \le 0.528$$

$$q_m(P_u) = Cp_u\rho_0\sqrt{\frac{T_0}{T_u}}, \quad (11)$$

where T_0 is the normal condition temperature [K], ρ_0 indicates the normal condition density [kg/m^3], C indicates the sonic conductance [kg.s/m^3], and P_u indicates the upstream side pressure inside the solenoid valve [MPa]. In addition, T_u is the air temperature [K], P is the downstream side pressure inside the artificial muscle [MPa], and γ is the critical pressure ratio.

3) Pressure change in the artificial muscle

Next, the compaction property of air, which is a characteristic peculiar to an air pressure system, is considered. A state equation can express the compaction property of a fluid. Equation (12) is obtained by differentiating and transforming this state equation. Then, the pressure change dP/dt inside the artificial muscle is expressed in terms of q_m, the inner volume of the artificial muscle V [m^3], and pressure P.

$$\begin{aligned}\frac{dP}{dt} &= RT\left(\frac{V}{\kappa}\right)^{-1} q_m - P\left(\frac{V}{\kappa}\right)^{-1}\frac{dV}{dt} \\ &= \frac{dP}{dt}\left(V, \frac{dV}{dt}, P, q_m\right),\end{aligned} \quad (12)$$

where R is the gas constant [Pa.m^3.Kg^{-1}.K^{-1}] and κ is the ratio of specific heat.

4) Generating contractile force in the artificial muscle

The pressure characteristic of the artificial muscle is expressed in equation (13) using the mechanical equilibrium model. The contractile force F [N] of the artificial muscle is expressed in terms of its internal pressure P and contraction x [m]. Note that G_1, G_2, and G_3 use equations (3), (4), and (5), respectively.

$$F(x,P) = \frac{PG_3(\phi_0) - G_1(\phi_0)}{G_2(\phi_0)} \quad (13)$$

5) Volume change in the artificial muscle

We modeled the change in the volume capacity according to the contraction of the artificial muscle. First, the artificial muscle becomes circular, as shown in Fig. 6. Then, the inner volume of the muscle V [m^3] can be expressed as follows:

$$\begin{aligned}V = \frac{l_0\pi}{4\phi_0^{\,3}}\Bigg[& d_0\phi_0^{\,2}l_0 + \left(d_0^{\,2}\phi_0^{\,2} + \frac{3}{4}l_0^{\,2}\right)\sin\phi_0 \\ & - \phi_0 l_0\cos\phi_0\left(l_0 + d_0\sin\phi_0\right) + \frac{l_0^{\,2}}{12}\sin 3\phi_0\Bigg]\end{aligned} \quad (14)$$

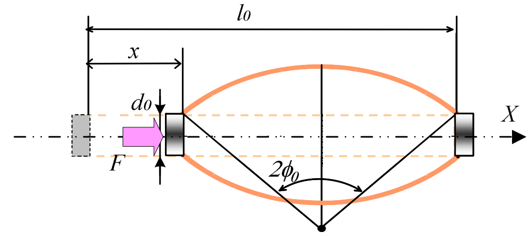

Figure 6. Shape model of the artificial muscle viewed along the *z*-axis

D. Load System Model of the Arm

First, we calculated the driving torque of the arm from the contractile forces F_1 and F_2 of the two opposing artificial muscles as follows:

$$\tau_d = (F_2 - F_1)r_p, \quad (15)$$

where r_p is radius of the pulley. Then, the angular acceleration of the arm is calculated from the forward kinetics:

$$\ddot{\theta} = \frac{\tau_d - \tau_m(\dot{\theta}) - \tau_l(\ddot{\theta}, \theta)}{I_1 + I_2}, \quad (16)$$

where I_1 is the inertia of the arm, I_2 is the inertia of the load [Nm.s^2], τ_l is the load torque [Nm], and τ_m is the damping torque of the MR brake [Nm].

IV. Generating Instantaneous Force

A. Method for Generating Instantaneous Force

In this chapter, we explain the generation of instantaneous force using the MR brake, as shown in Fig. 7. This MR method has three steps: 1) hold the joint rotation using the MR brake as a friction damper, 2) accumulate elastic energy in the artificial muscle on one side by applying air pressure, and 3) generate instantaneous force by releasing the MR brake.

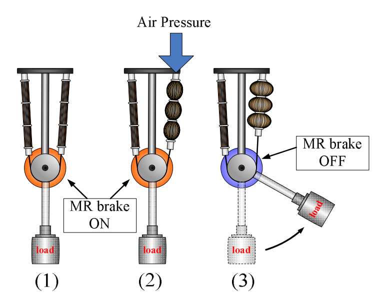

Figure 7. Generation of instantaneous force using the MR method

B. Selection of Initial Pressure for the Artificial Muscle

According to the MR method, the steady-state position of the arm depends on the initial pressure of the artificial muscle. No air pressure is added in the muscle during the manipulator drive, so it is necessary to calculate the initial pressure to raise the load to the desired arm angle. However, this pressure changes with changes in the volume and contractile force of the muscle.

Therefore, we obtained the experimental relationship between the volume and pressure of the artificial muscle. In the experiment, the initial pressure was applied to the artificial muscle, and the pressure and contraction were recorded. The volume of the artificial muscle was calculated from the contraction using equation (14).

The experimental result in Fig. 8 shows that the pressure is proportional to volume. This relationship does not depend on the initial pressure. We express this relationship using the following approximate equation, where P_0 is the initial pressure and V_0 the initial volume:

$$\frac{P-P_0}{V-V_0} = -0.0014 \tag{17}$$

According to this approximate equation, the initial pressure of the artificial muscle was calculated from the initial volume and the desired pressure and volume. The desired pressure was calculated from the desired angle and load torque using the mechanical equilibrium model. The desired volume was calculated from the contraction and desired angle using equation (14). Finally, the initial volume was calculated from the initial angle following the procedure used to calculate the desired volume.

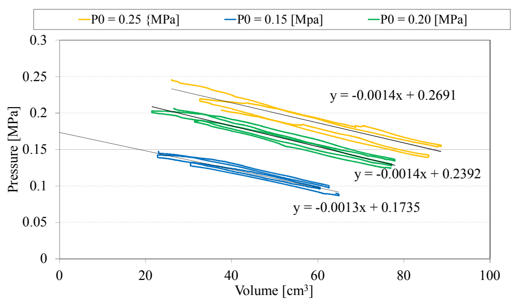

Figure 8. Relationship between pressure and volume of artificial muscle

C. *Instantaneous Force Generation Experiment*

In this section, we describe the generation of instantaneous force using the MR method. In the experiment, the initial pressure was calculated using equation (17) with the desired arm angle of 60[deg] and a load of 8.33 [N]. Fig. 9 shows the results obtained from the conventional method as well as the experimental and simulation results obtained from the MR method. The conventional method uses step input and torque feedback [15]. Table 2 shows the dead and rise times. The results show that the dynamic characteristics model of the manipulator effectively reproduces the manipulator system characteristics. Furthermore, we conclude that the initial pressure was correctly determined using equation (17). For the experimental results of the MR method, Table 2 shows that the dead time decreases by 68% and the rise time decreases by 12% when compared with the conventional method.

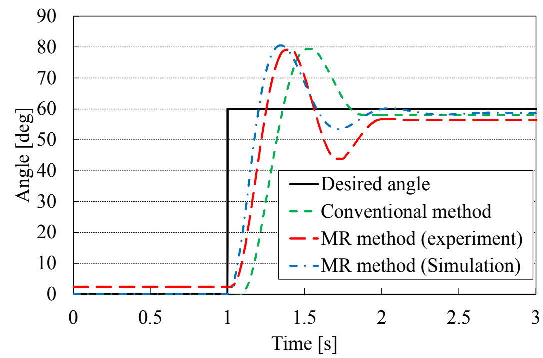

Figure 9. Experimental and simulation results

TABLE II. DEAD AND RISE TIMES

Term	Value	
	Dead time (s)	*Rise time (s)*
Step response	0.081	0.176
MR method (Experiment)	0.026	0.156
MR method (Simulation)	0.001	0.131

V. APPLYING EQUILIBRIUM FORCES FOR POSITION CONTROL

Although the manipulator generated instantaneous force, the initial pressure depended on the desired angle of the arm. Furthermore, this approach does not control the arm's joint stiffness after this motion. Therefore, we propose the application of an equilibrium force to the joint to achieve position control as shown in Fig. 10. With this method, the manipulator can control the arm position after an arbitrary instantaneous force is applied.

First, the manipulator generates instantaneous force using an arbitrary initial pressure. Next, air pressure is applied to the muscles to help control the arm position and joint stiffness. In the proposed method, additional air pressure was calculated using equations (1) and (2). However, we cannot simply apply air pressure after the arm reaches the desired angle because of the response delay of air pressure. Therefore, we determined the proper timing requirement as follows.

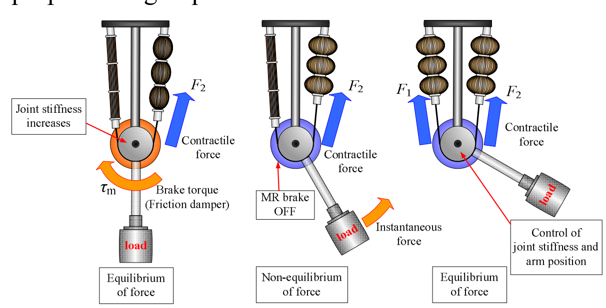

Figure 10. Applying equilibrium force for position control

A. *Pressure Timing*

As shown in Fig. 11, we calculated t_b from t_a and t_c to determine the proper time to apply addition pressure, where t_a

is the time when the arm reaches the desired angle obtained experimentally and t_c is the response lag of the pressure calculated using equation (18). In addition, both artificial muscles need different value of t_c, because these muscles are applied different pressure. Therefore, each t_c were determined by taking into account both muscles.

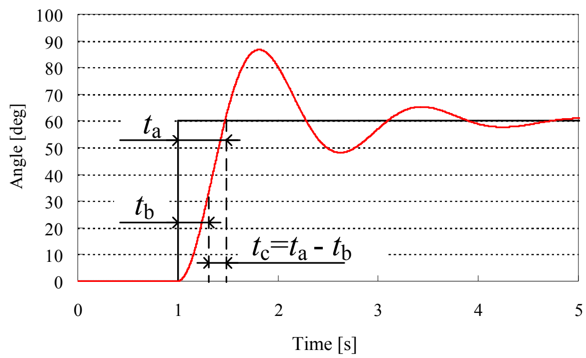

Figure 11. Presure timing

$$t_c = \frac{V_d - \frac{P_0}{P_d} V_0}{Q_m} \tag{18}$$

$$Q_m = 66.02 P_d + 11.141 \tag{19}$$

Here V_d and P_d are the volume and pressure of a muscle, respectively, when the arm reaches the desired angle with joint stiffness, and Q_m is the volume flow rate [m^3/s] of air from the solenoid valve to the muscle.

B. Experiment for Applying Equilibrium Forces for Position Control

We applied pressure to the muscles to control the arm position and joint stiffness after the generation of instantaneous force. In this experiment, we generated instantaneous force with an arbitrary initial pressure and then applied air pressure to the muscles in order to establish an equilibrium force and achieve the desired joint angle. The time of pressure addition is t_b, which is calculated in section V.A.

Figs. 12 and 13 show the experimental results for each initial pressure. The desired angles were 30 and 60 [deg], joint stiffness was 0.07 [Nm/deg], load was 8.33 [N], and initial pressures were 0.30, 0.35, and 0.40 [MPa]. From these results, we controlled the arm position by applying an equilibrium force to the joint for each initial pressure and desired angle. Furthermore, joint stiffness was controlled after applying an equilibrium state.

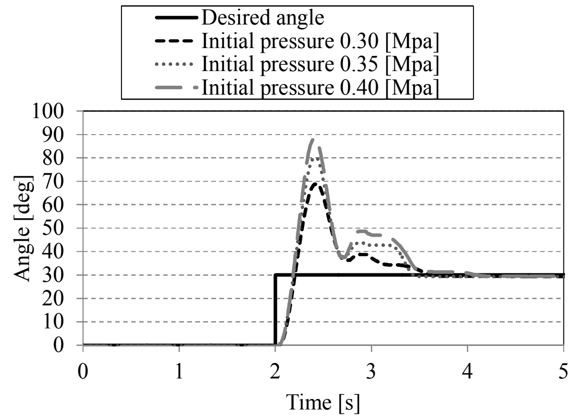

Figure 12. Experimental result of applying an equilibrium force (desired angle was 30 [deg])

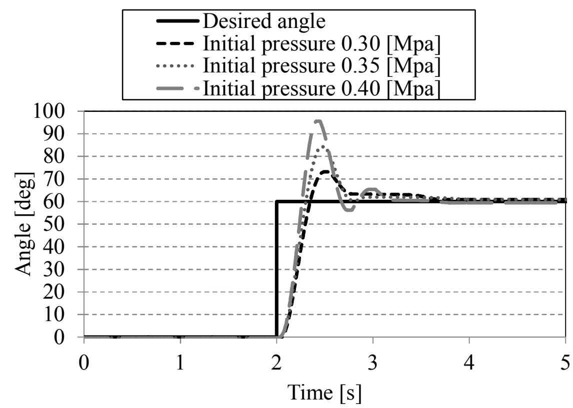

Figure 13. Experimental result of applying an equilibrium force (desired angle was 60 [deg])

VI. IMPEDANCE CONTROL WITH INSTANTANEOUS FORCE BY A 1DOF MANIPULATOR

A. Viscosity Control of MR Brake Using an Evaluation Function

As mentioned in section V, we were able to apply an equilibrium force to the joint and control the arm position after generating instantaneous force. However, we still experienced arm vibration and overshoot, as shown in Figs. 12 and 13. Thus, we controlled the arm vibration and overshoot using the MR brake as a variable viscosity damper by controlling its apparent viscosity. Then, we introduced a controller to change the apparent viscosity coefficient of the MR brake according to the motion of the arm.

We used the following evaluation function [16].

$$I(c_r, \dot{c}_r) = \int_{\theta_s}^{\theta_f} \{A(c_r\dot{\theta})^2 + B\dot{c}_r^{\,2}\} d\theta \tag{20}$$

Here A and B are weighting coefficients and $B = 1 - A$, c_r is the viscosity coefficient [Nm.s/deg], θ is angle of the arm [deg], θ_s is the vibration control start angle [deg], and θ_f is the vibration control finish angle [deg]. The first term is the element of interference of the brake torque to the arm, and the second term is the element of smoothness of change in the viscosity coefficient. In addition, using the variational method in equation (20) and solving Euler's equation, we obtain the following:

$$c_r(\theta) = \frac{c_s e^{-\theta_s V} - c_f}{e^{-\theta_f V} - e^{\theta_f V}} e^{\theta V} + \frac{c_f - c_s e^{\theta_f V}}{e^{-\theta_f V} - e^{\theta_f V}} e^{-\theta V}$$

$$V = \dot{\theta}\sqrt{\frac{A}{B}} \qquad c_f = c_r(\theta_f) \qquad c_s = c_r(\theta_s) \tag{21}$$

Here c_s is the initial value of the viscosity coefficient, c_f is the final value, and $c_s = 0$ [Nm.s/deg] and $\theta_s = 0$ [deg]. Using this function, we can control the viscosity of the MR brake according to the angle of the arm. Fig. 14 shows the relationship between the arm angle and the viscosity coefficient when c_f is 0.9 [Nm.s/deg], and θ_f is 60 [deg].

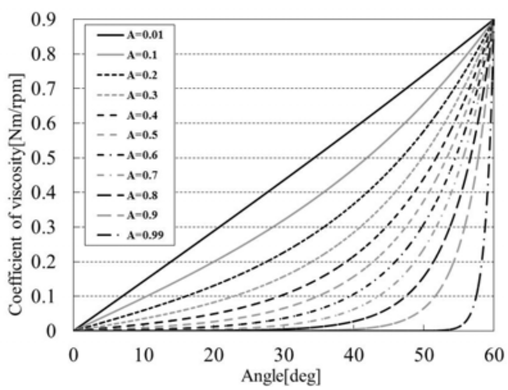

Figure 14. Relationship between arm angle and viscosity coefficient

B. Simulation for Viscosity Control Design

To use the evaluation function to control the viscosity of the MR brake, we must determine the parameters c_f and A. In this paper, we obtained these parameters by try and error using simulation. To this end, we simulated the MR method with the apparent viscosity control.

Fig. 15 shows the simulation results. The initial pressure was 0.35 [MPa], load was 8.33 [N], the weighting coefficient A was 0.7, and the final value of the viscosity coefficient c_f was 0.9 [Nm.s/deg].

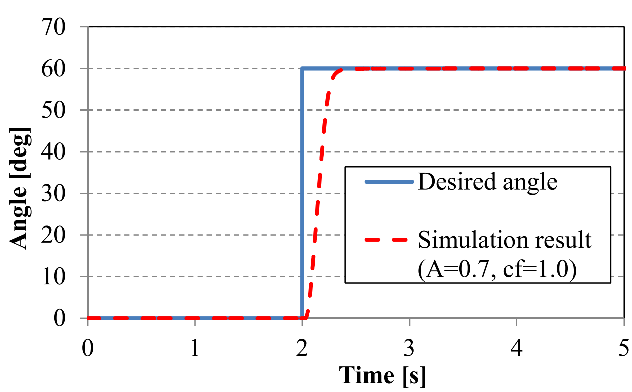

Figure 15. Simulation result with apparent viscosity control

C. Impedance Control with Instantaneous Force by MR Brake Using the Evaluation Function

We controlled the vibration and overshoot of the arm using the MR brake as a variable viscosity damper. We applied the arm position control described in section V here as well. We used the MR brake as follows:

- The apparent viscosity of the MR brake was controlled by the evaluation function. The weighting coefficient A was 0.7, and the final value of the viscosity coefficient c_f was 1.0 [Nm.s/deg], which were decided by simulation.
- The apparent viscosity of the MR brake was fixed at 0.1 [Nm.s/deg]. This condition was chosen experimentally to obtain stable response without vibration and overshoot of the arm.
- The apparent viscosity of the MR brake was fixed at 0 [Nm.s/deg].

The load was 8.33 [N], the desired angle was 60 [deg], and the joint stiffness was 0.07 [Nm/deg].

The experimental results are shown in Fig. 16. From this figure, the simulation results in Fig. 15 reproduce the experimental results. In addition, owing to the apparent viscosity control, the arm's vibration and overshoot decreased without suffering interference from the MR brake in the rise section. This result was compared with the results of the fixed apparent viscosity.

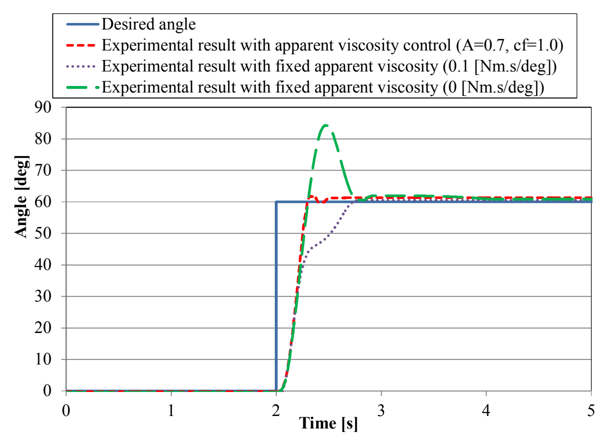

Figure 16. Experimental results with apparent viscosity control

VII. Conclusion

In this paper, we proposed a method for the generation of instantaneous force using an MR brake to produce a change in muscle stiffness. Using this method, we were able to demonstrate that the dead and rise times decreased compared with the conventional method with experiments and simulations.

We also applied an equilibrium force to the joint for position control. With this method, the manipulator can control the arm position after an arbitrary instantaneous force is applied.

We designed the apparent viscosity control of the MR brake using a nonlinear dynamic characteristics model of the manipulator in order to control the vibration and overshoot of the arm.

Finally, we controlled the vibration and overshoot of the arm by controlling the apparent viscosity of the MR brake using an evaluation function. As a result, the manipulator can control the arm position, joint stiffness, vibration, and overshoot using the instantaneous force.

VIII. Future Study

In future, we plan to calculate the initial pressure for the generation of instantaneous force in order to realize the desired speed and force. We also plan to develop a multi-DOF manipulator controlled by instantaneous force. In addition, we will test an arbitrary arm motion through experimentation.

References

[1] D. Braun, M. Howard, and S. Vijayakumar, "Optimal variable stiffness control: formulation and application to explosive movement tasks," *Autonomous Robots*, vol. 33, no. 3, pp. 237–253, 2012.

[2] T. Nakamura, N. Saga, and K. Yaegashi, "Development of Pneumatic Artificial Muscle based on Biomechanical Characteristics," in *Proc. IEEE Int. Conf. Industrial Technology (ICIT 2003)*, pp. 729–734.

[3] T. Nakamura and H. Shinohara, "Position and Force Control Based on Mathematical Models of Pneumatic Artificial Muscles Reinforced by Straight Glass Fibers," in *Proc. IEEE Int. Conf. Robotics and Automation (ICRA 2007)*, pp. 4361–4366.

[4] T. Nakamura, "Experimental Comparisons between McKibben type Artificial Muscles and Straight Fibers Type Artificial Muscles," in *Proc. SPIE Int. Conf. Smart Structures, Devices and Systems III*, p. 641424, 2006.

[5] H. Tomori and T. Nakamura, "Theoretical Comparison of McKibben-Type Artificial Muscle and Novel Straight-Fiber-Type Artificial Muscle," *Int. J. Autom. Tech.*, vol. 5, no. 4, pp. 544–550, 2011.

[6] G. K. Klute, J. M. Czernieki, and B. Hannaford, "McKibben Artificial Muscles: Pneumatic Actuators with Biomechanical Intelligence," *Proc. IEEE/ASME Int. Conf. Advanced Intelligent Mechatronics 1999*, pp. 221–226.

[7] C. P. Chou and B. Hannaford, "Static and Dynamic Characteristics of McKibben Pneumatic Artificial Muscles," *Proc. IEEE Int. Conf. Robotics and Automation 1994*, pp. 281–286.

[8] M. Kovac, M. Schlegel, J.-C. Zufferey, and D. Floreano, "A Miniature Jumping Robot with Self-Recovery Capabilities," *Proc. IEEE/RSJ Int. Conf. Intelligent Robots and Systems*, pp. 583–588, 2009.

[9] R. Niiyama, A. Nagakubo, and Y. Kuniyoshi, "Mowgli: A Bipedal Jumping and Landing Robot with an Artificial Musculoskeletal System," *Proc. IEEE Int. Conf. Robotics and Automation (ICRA 2007)*, pp. 2546–2551.

[10] B. J. Park, C. W. Park, S. W. Yang, H. M. Kim, and H. J. Choi, "Core-Shell Typed Polymer Coated-Carbonyl Iron Suspension and Their Magnetorheology," *ERMR08*, p. 102, 2008.

[11] H. Tomori, H. Maeda, and T. Nakamura, "Orbit Tracking Control of 6-DOF Lubber Artificial Muscle Manipulator Considering Nonlinear Dynamics Model," *Trans. Japan Soc. Mech. Eng.*, Series C, vol. 77, no. 779, pp. 2742–2755, 2012.

[12] H. Tomori, H. Maeda, and T. Nakamura, "Orbit Tracking Control of 6-DOF Lubber Artificial Muscle Manipulator considering Nonlinear Dynamics Model," *15th ROBOTICS Symp.*, pp. 429–435, 2010.

[13] H. Tomori, Y. Midorikawa, and T. Nakamura, "Construction of Nonlinear Dynamic Characteristic Model of Pneumatic Artificial Rubber Muscle Manipulator using MR Brake," *Journal of Intelligent Material Systems and Structures*, vol. 23, no. 9, pp. 408–415, 2012.

[14] JISB8390, Air pressure-Apparatus for compressive fluid-the test method of a flow characteristic, Japanese Standards Association, 2002.

[15] Y. Midorikawa and T. Nakamura, "Variable Rheological Joints Using an Artificial Muscle Soft Actuator and Magneto-Rheological Fluids Brake," *Intelligent Robotics and Applications 2009 (ICIRA2009)*, pp. 504–514, 2009.

[16] S. Nagai, H. Tomori, Y. Midorikawa, and T. Nakamura, "The Position and Vibration Control of the Artificial Muscle Manipulator by Variable Viscosity Coefficient Using MR Brake," *Proc. the 37th Annual Conference of the IEEE Industrial Electronics Society (IECON2011)*, pp. 307–312, 2011.